AFRL-RX-WP-TP-2009-4150

MOISTURE-INDUCED DELAYED ALUMINA SCALE SPALLATION ON A Ni(Pt)Al COATING (PREPRINT)

James L. Smialek

NASA Glenn Research Center

APRIL 2009

STINFO COPY

AIR FORCE RESEARCH LABORATORY
MATERIALS AND MANUFACTURING DIRECTORATE
WRIGHT-PATTERSON AIR FORCE BASE, OH 45433-7750
AIR FORCE MATERIEL COMMAND
UNITED STATES AIR FORCE

REPORT DOCUMENTATION PAGE

Form Approved
OMB No. 0704-0188

The public reporting burden for this collection of information is estimated to average 1 hour per response, including the time for reviewing instructions, searching existing data sources, searching existing data sources, gathering and maintaining the data needed, and completing and reviewing the collection of information. Send comments regarding this burden estimate or any other aspect of this collection of information, including suggestions for reducing this burden, to Department of Defense, Washington Headquarters Services, Directorate for Information Operations and Reports (0704-0188), 1215 Jefferson Davis Highway, Suite 1204, Arlington, VA 22202-4302. Respondents should be aware that notwithstanding any other provision of law, no person shall be subject to any penalty for failing to comply with a collection of information if it does not display a currently valid OMB control number. **PLEASE DO NOT RETURN YOUR FORM TO THE ABOVE ADDRESS**.

1. REPORT DATE *(DD-MM-YY)*	2. REPORT TYPE	3. DATES COVERED *(From - To)*
April 2009	Journal Article Preprint	01 April 2009 – 01 April 2009

4. TITLE AND SUBTITLE

MOISTURE-INDUCED DELAYED ALUMINA SCALE SPALLATION ON A Ni(Pt)Al COATING (PREPRINT)

5a. CONTRACT NUMBER
FA8650-06-2-5211 (AO 15)

5b. GRANT NUMBER

5c. PROGRAM ELEMENT NUMBER
62102F

6. AUTHOR(S)

James L. Smialek

5d. PROJECT NUMBER
2241

5e. TASK NUMBER
00

5f. WORK UNIT NUMBER
22410003

7. PERFORMING ORGANIZATION NAME(S) AND ADDRESS(ES)

NASA Glenn Research Center
Cleveland, OH 44135

8. PERFORMING ORGANIZATION REPORT NUMBER

9. SPONSORING/MONITORING AGENCY NAME(S) AND ADDRESS(ES)

Air Force Research Laboratory
Materials and Manufacturing Directorate
Wright-Patterson Air Force Base, OH 45433-7750
Air Force Materiel Command
United States Air Force

10. SPONSORING/MONITORING AGENCY ACRONYM(S)

AFRL/RXLMP

11. SPONSORING/MONITORING AGENCY REPORT NUMBER(S)

AFRL-RX-WP-TP-2009-4150

12. DISTRIBUTION/AVAILABILITY STATEMENT
Approved for public release; distribution unlimited.

13. SUPPLEMENTARY NOTES
PAO Case Number and clearance date: 88ABW-2009-1254, 31 March 2009.
This work was funded in whole or in part by Department of the Air Force contract FA8650-06-2-5211 (AO 15). The U.S. Government has for itself and others acting on its behalf an unlimited, paid-up, nonexclusive, irrevocable worldwide license to use, modify, reproduce, release, perform, display, or disclose the work by or on behalf of the U.S. Government.

14. ABSTRACT
Delayed scale failure was examined for samples of a Ni(Pt)Al-coated CMSX4 single crystal superalloy, cyclically oxidized at 1150^oC for 2000 hr. One sample exhibited accentuated coating grain boundary wrinkling, initiating local alumina scale spallation to bare metal, resulting in a final weight loss of 3.3 mg/cm^2. Spallation under ambient conditions was monitored with time after cooldown and was found to continue for times up to 24 h, producing up to 0.05 mg/cm^2 additional loss for each hold, and accumulating 0.7 mg/cm^2 (20% of the total) over the course of the test. After test termination, water immersion produced an additional 0.15 mg/cm^2 loss. (A duplicate sample produced much less wrinkling and time dependent spalling, maintaining a net weight gain). The results are consistent with the general phenomena of moisture-induced delayed spallation (MIDS) of mature, distressed alumina scales formed on oxidation resistant M-Al alloys. Relative ambient humidity is discussed as the factor controlling adsorbed moisture, reaction with the substrate, and hydrogen effects on interface strength.

15. SUBJECT TERMS

single crystal superalloy, local alumina scale spallation, moisture-induced delayed spallation (MIDS)

16. SECURITY CLASSIFICATION OF:

a. REPORT	b. ABSTRACT	c. THIS PAGE
Unclassified	Unclassified	Unclassified

17. LIMITATION OF ABSTRACT:
SAR

18. NUMBER OF PAGES
36

19a. NAME OF RESPONSIBLE PERSON (Monitor)
Mary Kinsella

19b. TELEPHONE NUMBER *(Include Area Code)*
N/A

Standard Form 298 (Rev. 8-98)
Prescribed by ANSI Std. Z39-18

i

Moisture-Induced Delayed Alumina Scale Spallation on a Ni(Pt)Al Coating

James L. Smialek
NASA Glenn Research Center
Cleveland, OH 44135

Abstract

Delayed scale failure was examined for samples of a Ni(Pt)Al-coated CMSX4 single crystal superalloy, cyclically oxidized at 1150°C for 2000 hr. One sample exhibited accentuated coating grain boundary wrinkling, initiating local alumina scale spallation to bare metal, resulting in a final weight *loss* of 3.3 mg/cm^2. Spallation under ambient conditions was monitored with time after cooldown and was found to continue for times up to 24 h, producing up to 0.05 mg/cm^2 additional loss for each hold, and accumulating 0.7 mg/cm^2 (20% of the total) over the course of the test. After test termination, water immersion produced an additional 0.15 mg/cm^2 loss. (A duplicate sample produced much less wrinkling and time dependent spalling, maintaining a net weight *gain*). The results are consistent with the general phenomena of moisture-induced delayed spallation (MIDS) of mature, distressed alumina scales formed on oxidation resistant M-Al alloys. Relative ambient humidity is discussed as the factor controlling adsorbed moisture, reaction with the substrate, and hydrogen effects on interface strength.

Introduction

Platinum modified aluminides are widely used as oxidation resistant coatings or bond coats for thermal barrier coatings (TBC) on single crystal superalloy turbine blades. They are noted for forming protective α-Al$_2$O$_3$ scales with greater longevity and adherence to the coating than for similarly formed aluminides without Pt. The exact role Pt plays is actively being studied. Early metallurgical treatises focused on the diffusional stability afforded by Ni(Pt)Al coatings due to the great affinity Pt has for Al and a decreased tendency to deplete Al by interdiffusion with the substrate [1 Schaeffer 1989].

These and related phenomena have been detailed in many subsequent studies by Gleeson et al., as recently reviewed in a comprehensive treatise [2, Gleeson 2009]. Here it is described that while Pt actually increases D_{Al}, it reduces a_{Al}, thus influencing uphill diffusion of Al from the substrate into a Ni-Pt-Al coating and countering the detrimental Al depletion caused by interdiffusion [3, 4 Gleeson 2004, Copland 2005]. Pt additions also broaden the field for stable alumina formation on a ternary oxidation map to include lower Al contents and phases (i.e., reduces the critical Wagner solute content for healing scales, N_{Al}^{*}) [2]. This stems from the tendency for Pt to replace Ni in the lattice and present a reduced effective Ni/Al surface ratio for transient oxidation. It also results from the reduced oxygen solubility/permeability when Pt is added to Ni-Al alloys, thus discouraging detrimental internal oxidation with respect to an external healing layer of alumina [3 Gleeson 2004]. These beneficial effects would be magnified from potential Pt surface segregation [5 Gleeson 2007].

Other beneficial mechanisms are suggested by the compelling observations that Pt diminishes sulfur surface and interfacial segregation. It consequently encourages stronger interfacial strength (toughness) and reduces interfacial void formation resulting from the low surface energy of sulfur [6-10 Cadoret, et al. 2004, Hou and McCarty 2006; Hou and Priimak 2005, P.Y. Hou and V.K. Tolpygo 2007, Monceau 2009]. Another contributing factor is the exceptionally strong bond formed between pure Pt and Al atoms in Al_2O_3 [11-13 Anderson, et al 1987, Yu and Hou 2007, Gauffier and Hou 2007]. However, Pt enrichments do not seem to dominate the actual alumina - Ni(Pt)Al interface for β-NiAl [7 Hou and McCarty 2006]. In fact, the Pt effects on segregation, void growth, and interface strength are quite complex and depend considerably on the Ni-Al stoichiometry and alloy phase, as summarized in the recent review of interfacial segregation by Hou [14 Review 2008]. In general, void formation and sulfur interfacial segregation become more appreciable as the Al content is reduced. Here Pt may benefit depleted β-NiAl by producing an Al interface enrichment, allowing the preferred behavior more typical of the stoichiometric alloy. Additionally, the crystallographic orientation of β-NiAl has been shown to influence both sulfur segregation and the degree of interfacial void formation [8 Priimak and Hou 2005], remarkably allowing voids to form on low indice planes of even desulfurized or Y-doped Ni40Al5Cr [15 Hu et al. 2009].

Despite outstanding oxidation behavior as a bulk material, an issue specific to aluminide coatings is a propensity to deform, especially when cycled. In one description, this phenomenon (ratcheting) [16 He, Evans, Hutchinson 2000] results from the CTE mismatch with the substrate and an irreversible creep strain that occurs during cooling. This roughness, coupled with as-processed grain boundary ridges in the coating, produces stress concentrations and a normal tensile stress to the scale. Preferred failure sites and interface crack initiation under a TBC are the result. Thus, scale adhesion remains a concern and is especially critical for TBC applications.

While alumina scale adhesion is normally discussed in terms of sulfur content and interface segregation, along with reactive element and Pt contents, an auxiliary chemical factor exists in the environment, moisture. Generally, moisture effects are observed for at-risk scales, i.e., those that have just enough adherence to be retained by a conventional thermal cycle stress, but may delaminate upon extra duress. Thus, for example, scales formed at intermediate sulfur contents or thick scales with exceptionally high strain energies may be especially susceptible to moisture effects. These phenomena have been directly illustrated for various alloys in a number of early studies [17-21 Smialek 1978, Smialek 1986, Sigler 1993, Smith 1995, Janakiraman 1999]; the results and viewpoints from our laboratory have been summarized in [22,23 Smialek TM 2005, les Embiez 2008].

One aspect of moisture-induced delayed spallation (MIDS), since the scale has been initially retained upon cooldown, is the time dependent nature. MIDS is most evident when the spallation event is intentionally triggered by the initial exposure to moisture (e.g., moist breath or water immersion). However, holding the material at ambient atmospheric humidity or submerged in water is known to cause progressive time dependent delamination of alumina scales, proceeding for times up to 24 hr. [24,25 Clarke, C and T 1997, Morscher 2002]. Indeed, interfacial buckle growth has been directly monitored for a sample while observed under a microscope [26 Tolpygo and Clarke, Mat Sci Eng 2000]. The implications on TBC failure have

been drawn, and many studies extend the concept to include unintentional [24,26-29 Clarke, C and T, 97, Sergo and Clarke 1998, Peng and Clarke 2000, Smialek ACerS 2002] or intentional [30 Smialek JTST 2004] moisture-assisted TBC delamination. The latter recently includes videos of water-induced failure of TBC's on coupons [31,32 Scripta Video 2008, Rudolphi 2008] and on commercial turbine blades [33,34 Cadoret 2008, Smialek 2009].

Returning to the specific case of aluminide coatings, oxidation in 0.1 and 0.3 atm H_2O air has been found to increase the amounts of weight loss in 1100^oC cyclic tests of simple aluminide coatings with increase in $p(H_2O)$ [21,35 Janakiraman 1999, Maris-Sida 2003]. However the same effect was not especially evident for the more oxidation resistant Ni(Pt)Al Pt-modified coatings. One can expect that this effect will be enhanced in proportion to the amount of surface deformation by rumpling and degree of cyclic oxidation.

The purpose of the present paper is to again call attention to the time dependence of alumina scale spallation. This occurs when mature scales are subjected to normal laboratory room conditions at ambient temperatures and local humidity, as normally encountered during conventional sample weighing and examination procedures. Attention is paid to coating grain boundary ridges and associated deformation, since spallation appears to be closely related to such features. The material studied was a widely-used Ni(Pt)Al bondcoat on single crystal superalloy substrates. Such phenomena become important for turbine applications in both quantifying oxidation degradation and for understanding the potential for delayed thermal barrier coating (desktop) failures.

Experimental

Coupons of superalloy (CMSX4) were machined from ~ 1/8 x 1 x 6" cast single crystal slabs (PCC) and coated with a commercial Ni(Pt)Al aluminide coating (MDC-150L, Howmet Corporation, Whitehall, MI.), *all from the same ingot and coated in the same batch (?).* (They were provided by Dr. Kang Lee, Rolls-Royce Corp., Indianapolis, IN, as part of a Materials Availability Initiative (MAI) study, sponsored by WPAFB, Donna Ballard, Program Manager). Briefly, the Pt was electrodeposited to a thickness of about 5^+ μm and aluminized in a low activity CVD process.

The samples were approximately 3.2 mm x 1.27 cm x 2.54 cm, with a hanger hole at one end, with approximately 9.1 cm^2 surface areas, weighing approximately 9 g each. They were ultrasonically cleaned in detergent, rinsed in water then ethanol, and dried. Samples were cyclically oxidized at 1150^oC, suspended by Pt hang wires, in a vertical, 6 alumina tube furnace, using a 60 min. heating cycle and a 20 min. cooling cycle for 2000 cycles. Cycling was accomplished by a pneumatic cylinder actuated assembly, controlled by electronic timers and counters. The furnace control temperature was constant, remaining within 1-2 C^o throughout the test. Hot zone variations ranged up to 5 C^o, depending on the individual tube. During each cooling cycle, the samples were retracted into a baffled chamber above the furnace, providing some barrier to direct thermal drafts. However, the environment was still relatively warm and dry, maintaining ~100^oC.   (For example, the chamber equilibrated at 105°C when the furnace lab air was 17°C or 124°C when the lab was 22°C.

Samples were weighed on an analytical balance over a graduated time schedule (1, 2, 5, 10, 20, 40, 60, …500, 550, 600, …1000, 1100, 1200, …2000 hr.). It is shown that this weighing schedule automatically provides exposure to a considerably higher relative humidity of the balance room. Since we are concerned with small amounts of additional spallation, occurring well after the cooling cycle, some discussion about measuring small weight changes is warranted. The balance sensitivity was 0.01 mg. However drift was much greater than this, depending for example on the ambient temperature, humidity, and, more importantly, on any thermal instability impacting the balance. The latter was partially addressed by an outer plexi-glass balance chamber (with access doors) surrounding the balance. Also, it was insured that the samples were fully cooled to ambient conditions (generally 15 min. or longer) before weighing (except for the special time-dependent tests discussed later).

A key step was to always re-zero the balance and obtain a calibration weight from a 10.00000 gm standard before each weight. This provided an unchanging reference mass against which any balance drift changes could be corrected for each individual measurement. Over the course of the 9 month test, the standard varied over a maximum range of 0.25 mg (~10.00008±0.00004 g average of about 110 measurements made over the duration of the test). For the 9 cm^2 samples used, the standard deviation of this repeated reference measurement would translate into a standard error of sample measurement of less than *0.005 mg/cm^2*.

After 750 cycles, when spontaneous spallation became apparent, multiple measurements were made over time to track any delayed spallation. For special time-dependent tests, weights were recorded for the first few minutes and hours, up to one day at ambient. Exposure to additional moisture (1-h water immersion) was performed at the end of the 2000 h test. Optical macrographs were obtained over the course of the test to document overall spallation patterns, while SEM/EDS was performed at the end of the test to reveal scale morphology and spallation patterns.

Results

The coatings were characterized by electron microprobe [36 Nesbitt 2008, communication]. The as-coated thickness, measured from the surface to the included alumina particles (from the initial grit blast surface prep), was $37 \pm 1\mu m$. Composition varied somewhat across the layer, nominally 50Ni - 8Co - 8Pt - 35Al - 4Cr – 0.5Ta (atomic %). Some of TCP phases lie within the coating, above the diffusion zone + TCP region. The latter was an additional 30 µm thick. The surface morphology can be seen in Figure 1, where grain boundary ridges can be discerned. These are typical of the often observed grain boundary ridges associated with CVD Ni(Pt)Al coatings (9,35 Hou and Tolpygo 2007, Maris-sida 2003). Crystallographically aligned surface striations and pits are also evident, presumably an artifact of the CVD process and environment. The EDS response of the overall coating, grain interiors, and grain boundaries was generally similar, showing basically uniform amounts of Ni, Pt, Al with a small amount of Cr, Fe, and Co, Figure 2.

Weight change and delayed spallation. The overall total 1150°C weight change behavior (due to normal cycling and any delayed spallation) is shown in Figure 3. The response of sample 1150-2 indicates a fairly typical increase to a maximum of 0.8 mg/cm^2 at 460 h, followed by a more or

less linear loss rate to -3.3 mg/cm^2. A nominally duplicate sample, 1150-4, increased to a maximum of 0.5 mg/cm^2 at 1350 h and displayed a very small spallation rate afterwards, ending at +0.4 mg/cm^2. (Four other duplicates, tested for times between 100 - 1000 hr as part of a broader study, showed a similar range of responses). Thus, higher growth rates and higher spallation rates are noted for sample 2 compared to sample 4 and appear to represent a range of behavior for this class of material.

The accrued amount of additional delayed spallation, obtained by holding the samples at ambient humidity for up to a day, is shown in Figure 4. These values are separate from any spallation that occurred during normal cycling, the latter being determined by initial weight measurements immediately upon removal from the furnace. The plot begins with data only after 750 cycles, when spallation became more visually pronounced. As with the total weight change in Figure 3, it is seen that sample 2 produces a noticeable, steady-state spallation, while sample 4 appears very benign. These curves imply a constant amount of delayed spallation for each weighing cycle. Accordingly, the amount of delayed spallation recorded each time the samples are removed from the furnace test is shown in Figure 5. On average, the amount lost per inspection period is 0.04 mg/cm^2 for sample 2 and 0.00 mg/cm^2 for sample 4. Because of these relatively small amounts, there is considerable scatter in this plot. There is very little change for either sample, from 750 hr to the end of the test.

The actual time dependence of the delayed spallation is shown for a number of inspection periods in Figures 6 and 7 for samples 1150-2 and 4, respectively. Here the time axis is shown as $t^{1/2}$ in order to compress the sparse data obtained after one hour hold time. The exact starting time is problematic. Ideally, one would measure an initial weight as soon as the sample is removed from the warm, dry furnace area, reaching about 100-120°C. On one hand, weighing immediately would allow this residual heat in the samples to affect the balance. But on the other hand, longer preliminary cooling in ambient would allow more delayed spallation to occur undetected. To assess the residual retained sample heat problem, an unoxidized control sample was weighed as a function of time from the cooling chamber, allowing various times of cooling before beginning the weighing. With only 15 sec of cooling, the time it takes to remove the sample and bring it to the balance, the perceived weight was found to deviate negatively a maximum of ~0.5 mg, before decaying away over the next 15 min. However, allowing for a 2 minute cool, this deviation was only ~0.2 mg, equivalent to ~0.02 mg/cm^2 error. This latter procedure was adopted as an acceptable compromise. The residual error applies primarily to the first reading, essentially removed by the next re-calibration for the 10 g standard, also effected by the thermal effect.

Acknowledging these uncertainties for low initial readings, it is evident from Figure 6 that a progression of time delayed spallation was observed for sample 2 for times up to 1 day. Furthermore, the magnitude and decay rate was, for the most part, reasonably similar for the seven plots shown, over 1000 hr of test time. Any initial rise in weight was due to the thermal effect on the balance. The absence of significant time delayed spallation for sample 1150-4 in figure 7, relative to ±1σ, is consistent with the all data shown previously for this highly oxidation resistant sample. This sample was always weighed after sample 1150-2, with all readings effectively re-calibrated by the 10 g standard weight. It therefore shows little thermal transient effects even for the first few minutes.

Morphology. Early on in the study, it was noted that the coatings exhibiting higher growth rates and spallation also exhibited a roughened surface texture early in the testing. Figure 8 shows an optical macrograph of the two samples, obtained under oblique lighting, after 200 1-h cycles. It is clear that sample 2 is significantly rougher than sample 4, especially regarding the grain boundary region. Figure 9 presents optical micrographs of the surface showing detail regarding the specific spallation sites. Here sample 2 reveals delaminated scale fragments and exposed bare metal, both in the immediate vicinity of coating grain boundaries. These features increase with exposure time, eventually exhibiting a distinct blue-green tint to some scale fragments. By comparison, sample 4 is relatively featureless, showing a less contorted landscape with more shallow grain boundary features. There is only limited indication of scale delamination or exposed metal and relatively slight changes with continued cycling. These initial features are believed to coincide with the wide divergence in behavior in Figures 3-7.

The macrographs in Figure 10, obtained after 2000 1-h cycles, confirm a higher degree of scale spallation to bare metal for sample 2. Numerous and larger spallation features are noted compared to only a few minute spall segments for sample 4. The spalled regions extend to about 1 mm long for sample 2, but only as much as 0.1 mm for sample 4. Water immersion produces noticeable additional spallation for sample 2, but not for sample 4. Again, it is believed that the increased spallation arose from the stress concentrations at the large curvatures of the rumpled Ni(Pt)Al coating grain boundaries.

These results are augmented by SEM/BSE/EDS studies. The low magnification BSE micrographs in Figure 11(a) reveal a large (brightest) area of spalling to bare metal for sample 1150-2, with widely varying degrees of intensity in the surrounding intact scale regions. Detailed analyses reveal typical scale-metal imprints in the spalled regions and mixtures of, presumably, Al_2O_3 (dark), $(Ni,Co)(Al,Cr)_2O_4$ (grey), and dispersed $(Ti,Ta)O_2$ (bright) oxides. While there is some indication of layered scales, the various regions also probably relate to areas with different histories of spalling and re-growth. Characteristic EDS spectra are shown in figure 12 for an exposed (Ni,Co,Cr,Al,Pt,W,Ti) metal region and (Ni,Al,O) spinel scale region.

Very little spalling was observed for sample 1150-4, Figure 11(b), showing a very uniform backscatter response. However, some scale cracking, without appreciable spallation, occurred predominantly at wrinkled coating grain boundaries. The scale was consistently Al_2O_3, Figure 12, with only a fine dispersion of Hf-rich oxide particles decorating the ridge structure. Numerous details of the SEM characterization of both samples will be presented in a companion paper [37 Garg 2009].

Discussion

The weight change data shown above indicates that a measurable amount of additional (delayed) scale spallation is possible during typical cyclic oxidation tests of a commercial oxidation resistant coating. The phenomenon takes place simply by exposing samples to a higher relative humidity away from the warm 'cooling' chamber of the furnace test. Not only does a relatively

consistent amount of additional spallation occur, but it follows a somewhat similar trend over the span of a day, and perhaps longer. The final spallation event is due to water immersion at the end of the test.

These observations are consistent with the overall mechanism of moisture-induced delayed spallation (MIDS), often observed for partially adherent alumina scales. These scales are adherent enough to withstand some degree of thermal cycling, when retained in dry environments during cooldown. This phenomenon may result from various combinations of the following factors: 1) a modest sulfur content (0.2-1 ppmw), where partial adherence is commonplace, 2) an insufficient or non-unifom distribution of reactive elements, 3) a high degree of strain energy (i.e., thick scales), and 4) stress concentrations (due to rumpled or rough surfaces). In the present case, a high degree of adhesion is imparted by the Pt alloying addition. However, there is apparently a range of behaviors that stem from the surface roughness at the coating grain boundaries. Lower overall growth rates and higher adhesion results for the coatings that were processed relatively flat and remained smoother.

Moisture effects on aluminide coatings. A single early moisture test of oxidized bulk Ni42Al in saturated 80°C air resulted in a loss of 0.1 mg/cm^2 (after an 1100°C cyclic test in which the samples gained less that 1 mg/cm^2 over 500 1-hr cycles) [17 Smialek 1978]. The deleterious effects of continuous exposure to moisture is significant during 1100°C cyclic oxidation of NiAl diffusion aluminide coatings on PWA 1480 (21 Janakiraman, 1999), losing about 60 mg/cm^2 after 1000 1-hr cycles in 0.1 atm P(H$_2$O), as compared to just 3 mg/cm^2 for oxidation in dry air. A similar but less severe effect was reported for the same coating on Rene´N5 (35 Maris-Sida, 2003), exhibiting a loss of 1 mg/cm^2 in wet air compared to only 0.1 mg/cm^2 in dry air. However, moisture effects for Ni(Pt)Al coatings on Rene´N5 were not very apparent. Here a gain of about 0.2 mg/cm^2 was achieved after 2000 1-hr cycles in 0.1 atm P(H$_2$O), as compared to a gain of 0.6 mg/cm^2 for oxidation in dry air. Only an increase in the amount of spinel at the gas surface was observed. The general trend was discussed in terms of hydrogen-induced defects in NiO and Al$_2$O$_3$, resulting in faster outward transport of Ni. It was also suggested that that spinel formation may also have been initiated by moisture-induced cracking and re-oxidation, as observed in the present study, where moisture was not present during oxidation.

Moisture effects are confirmed by Pint [38 2006] in tests of aluminide coatings and bulk β-NiAl, (plus γ/γ´ and NiCrAlY) tested in 10% water vapor. In general the data suggests that moisture can affect spallation for aluminides, especially for alumina scales having less than optimum scale adhesion (no alloying elements of Pt, Hf, Y etc.). As in the above, water vapor was maintained in the oxidation exposure such that these samples were automatically subjected to moisture induced effects before removing them to the balance environment. Thus it is envisioned that continuous thermogravimetric analysis (CTGA) [39 Monceau] in moist environnments might be a particularly useful test for more precisely determining the time-dependent nature of this phenomenon.

Delayed failure and Ni(Pt)Al bond coat oxidation was also implicated in TBC failure modes (40 Tolpygo, Clarke, Murphy 2001). Here the time dependence of TBC failure was pointed out, necessitating a 2-hr hold time at room temperature between cycles to allow the effect to run its course. While differences in kinetics and TBC lifetimes were noted between as-aluminized and

grit blasted (smoothed) bond coats, both failure loci exhibited substantial amounts of interfacial scale-metal debonding. Thus time dependent moisture-induced scale failure probably played some role for both surface conditions, even though TBC failure initiated at edges.

Since moisture interfacial failure has been implicated in these and the present studies, it is informative to examine an analogous study using finely controlled relative humidity effects [41 Shiue 2006]. This work measured the interfacial shear strength of a polymeric coating on glass fibers as function of exposure time, relative humidity (RH), and temperature. Here the time factor is related to moisture transport through polymeric interfaces as opposed to hydrogen diffusion at the scale metal interface, as discussed later. But although the controlling mechanisms differ from delayed spallation in the atomistic details, it is still illustrative to examine the formal dependencies. Here, interface strength was found to decay exponentially with time and to be reduced as the relative humidity increased, as $(RH)^{2/3}$. Similar asymptotic spallation kinetics were presented in Figure 6 for delayed scale spallation. A connection to relative humidity is thus discussed below.

Our present study was performed in laboratory air. There was no intentional increase in moisture content during the delayed spallation that occurred during sample weighing. What did increase was the relative humidity in removing the sample from the cooling baffle above the furnace to ambient conditions. In order to assess relative humidity effects, we examine temperature dependent saturation values and typical relative humidity levels reported for our area. The saturation level of moisture can be estimated from the relation [41,42 Shiue 2006; Keenan]:

$$P_{H_2O,sat'n}(T) = P_{H_2O,sat'n}(0^\circ) + k\left[\frac{T}{100^\circ C}\right]^n \tag{1}$$

where, $k = 0.0987$ MPa
            $n = 3.36$
$P_{H_2O,sat'n}(0^\circ) = 0.00198$ MPa

The saturation pressure (100% RH) is shown in Figure 13 as a function of temperature. Thus, at 0°C the saturation moisture content in the atmosphere is 0.00198 MPa, (~0.020 atm). For the local environment, weather almanacs report an average high relative humidity (RH) of 85% for mornings in August, shown as the second curve, giving 0.00213 MPa (~0.021 atm) at the average August temperature of 21°C.

   (see for example, http://www.cityrating.com/cityweather.asp?city=Cleveland)

However, the cooling chamber above the furnace is about 100°C, while the total moisture content is fixed by that in the ambient. At 100°C, the saturation level rises to 1 atm (0.1013 MPa), or estimated from eqn. 1 as 0.1007 MPa. The relative humidity of each location can then be estimated from:

$$\text{RH}_{\text{balance}} = \frac{P_{H_2O,21^o}}{P_{sat'n,21^o}} = 0.85 \qquad (2)$$

$$\text{RH}_{\text{chamber}} = \frac{P_{H_2O,21^o}}{P_{sat'n,100^o}} \qquad (3)$$

Combining eqn. 1, 2, and 3, one determines that the relative humidity in the 100°C cooling chamber is only 2.1%. Consequently, removing a sample from the cooling chamber to the ambient at 85% essentially exposes the sample to a 40x increase in relative humidity. (At the 1150°C test temperature, the saturation value is 361 MPa (3570 atm), or $1.7x10^5$ times that at 21°C, producing extremely low relative humidity during oxidation and no expected moisture effect.) The same exercise can be performed for colder, dryer months, but with similar conclusions.

One working hypothesis of moisture-induced delayed spallation is based on the direct access of moisture to the oxide-metal interface from cracks or pre-existing partial spallation [22,43 Smialek, JOM 2006, TM 2005]. This allows reaction of water vapor with aluminum in the alloy to form aluminum hydroxide and hydrogen according to the reaction:

$$\text{Al}_{\text{alloy}} + 3(H_2O)_{\text{ads}} = \text{Al(OH)}_3 + 3H^+ + 3e^- \qquad (4)$$
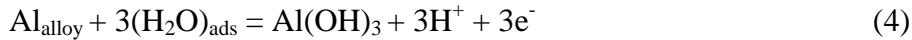
Hydrogen embrittlement of an at-risk interface is postulated as the root cause of moisture induced delayed spallation. So the question arises as to whether relative humidity or the partial pressure of water vapor is controlling the amount and activity of $(H_2O)_{\text{ads}}$ and the production of hydrogen at the interface. Unlike high temperature effects where P_{H2O}/P_{O2} affects oxide stability, the previous analysis suggests that relative humidity may play a role for MIDS, at least in these regimes of low moisture contents <0.1 atm. As a general rule it has been shown that the amount of adsorbed water on metal surfaces is indeed directly related to RH, such that ~0.1 monolayer can be expected for RH = 2% and ~5-10 monolayers for RH = 80% [44 Kucera 1989]. That is to say, the amount of adsorbed moisture would be predicted to increase 50-100x upon removing the sample from the furnace cooling chamber. Thus a commensurate increase in $[H]^+$ is obtained according to eqn. 4, along with a corresponding decrease on interfacial strength.

<u>Roughness effects on spallation</u>. Surface roughness has been associated with bond coat oxidation failures and can be discussed in a hierarchy of severity. Broadly speaking, terms like wrinkling, ratcheting, ridges, and rumpling describe undulations of an increasing magnitude (or wavelength). Wrinkling applies to the surface instability resulting from isothermal lateral growth within the scale adhered to a metal that creeps; this occurs on a fine scale (45 Tolpygo 1998). Ratcheting applies to a similar instability caused by thermal expansion mismatch stresses during cycling and an irreversible plastic strain that occurs on cool down as the rigid low expansion oxide scale forces the metal to extend (16 He, Evans 2000). Ridges are the β-NiAl grain boundary surface hillocks (and valleys) resulting from the diffusion aluminizing process. And rumpling is a variation due to a non-uniform dispersion of β-NiAl to γ′-Ni3Al phase transformations resulting from interdiffusion and aluminum depletion, often associated with

grain boundaries (46, 47 Tolpygo and Clarke, Acta mat 2000 and 2004). Other strain instabilities, such as reversible martensitic transformations in Ni(Pt)Al (48-50 Zhang 2003; Chen, Hemker 2003, Pan, Hemker 2003) have been suggested as factors encouraging scale and TBC failures. However, bond coat grain boundary topographical excursions appear to be playing the major detrimental role here, with the stress concentrations at sharp curvatures initiating scale failure. This grain boundary effect, however, may work in synergy with these other mechanisms.

In any case, *variations* in Ni(Pt)Al coating performance, based on surface roughness (rumpling and grain boundary ridges), have been observed previously, analogous to the present situation (51 Tolpygo, Clarke, 2003). Here performance was categorized by TBC cyclic life, though connections were drawn to bond coat oxidation properties and the propensity for scale spallation to initiate at grain boundary ridges. Again, no underlying cause for the variations was discovered, but implications were drawn regarding deleterious grain boundary chemistry. This unfortuitous occurrence of grain boundary ridges and their role in scale and TBC spallation has been expounded further (52 Tolpygo, Clarke, 2005). Here the features were correlated by coating batch, though not specifically connected to the causative factor. Indeed, others have correlated TBC life with bond coat roughness and the rate of rumpling, both being a direct function of scale thickness (oxidation time) and lateral growth strains (53,54 Sridharan, et al, 2005; Wen, Jordon, Gell 2006). Variation in Ni(Pt)Al cyclic behavior can be seen in other studies (55,56 Vialas and Monceau 2006, 2007, Murphy 2008).

In any event, the wide difference in behavior between the two samples provides a troubling subtext to the moisture effects, at least at this elevated test temperature. At this time there is no obvious difference between the two coatings. They were nominally processed as replicates in the same coating runs. Since no characterization was performed during the individual processing steps, it is impossible to back trace potential factors, such as initial sulfur content. It can only be said that the two samples exhibit an apparent difference in surface roughness early on in test, due in part to the as-coated topography. These Ni(Pt)Al grain boundary ridges initiate scale spallation and result in much less protective behavior for sample 1150-2, although some indications for boundary wrinkling and spalling has become apparent for sample 1150-4 after 2000 cycles.

In the present work, this propensity for spallation is also exhibited in the degree of moisture induced delayed spallation. This is consistent with the overall attributes of MIDS, which require partially compromised scale adhesion before becoming active. Some access to the oxide-metal interface is also required, as would happen for the grain boundary wrinkling-induced fractures. The latter is only enabled by the substantial stored strain energy resulting from extensive oxidation. Lower temperatures would result in reduced wrinkling and considerably less spallation over much longer times.

The appearance of ridge-related spallation as early as 200 hr (Figure 9) may play some role in initiating delayed (desktop) failure of EB-PVD TBC's on Ni(Pt)Al coated Rene′N5 discs [31 Scripta Video 2008]. Here, similar 1150°C furnace cycling produced TBC failure at the scale-metal interface between 220-420 hr. However, water drop induced TBC failures were produced at just 260-300 hr, compared to 750 hours when these effects on scale spallation began to be

quantified in the present study. In one sense the TBC can be seen to restrain scale spallation for a while, since it is behaving as a rigid top layer and would serve to reduce rumpling. In another sense the TBC CTE mismatch contributes to the strain energy driving spallation of the TBC and attached scale. In general terms, moisture can be seen as a factor for TBC failure when it has access to and weakens the metal interface of highly stressed scales.

Concluding Remarks

Commercial platinum aluminide coatings were oxidized at 1150°C for 2000 1-h cycles. Weight change was monitored throughout the test and occasionally as a function of hold time under ambient, room temperature conditions. The relative humidity was estimated to be increased by a factor of 40 from the warm 'cooling' chamber of the furnace to the ambient balance conditions. The degree of adsorbed moisture and potential interfacial hydrogen production was proposed to increase proportionally.

Moisture-induced delayed spallation was found to proceed, at a decreasing rate, for up to one day after cooldown. This occurred preferentially for the overly stressed scale regions on the sample having grain boundary ridges typical of aluminide coatings, progressing after extensive pre-cycling. This is consistent with many previous observations of moisture enhanced or delayed scale spallation for conventional aluminides and single crystal superalloys. But it is less widely appreciated that such phenomena may also occur for commercial platinum aluminide coatings. This has implications for delayed TBC failure (desktop spallation) when platinum aluminide bond coats are used.

Another practical ramification is to recall that cyclic data is subject to a certain amount of variation based on specific experimental protocols: e.g., the temperature reached each cooling cycle, the frequency of inspection, and the residence time at ambient conditions. Some attention to consistent weighing procedures is again noted and the utility of controlled humidity environments is acknowledged.

Acknowledgements

References

1. J.C. Schaeffer, G.M. Kim, G.H. Meier, and F.S. Pettit, in *The Role of Active Elements in the Oxidation Behavior of High Temperature Metals and Alloys*, E. Lang, ed., Elsevier (1989), 231-267.

2. B.Gleeson, N. Mu, and S. Hayashi, J. Mater. Sci. (2009) in press.

3. B. Gleeson, W. Wang, S. Hayashi, and D. Sordelet, Materials Science Forum, 461-464 (2004) 213-222.

4. E. Copland, Thermodynamic Effect of Platinum Addition to β-NiAl: An Initial Investigation. NASA CR 2005-213330

5. F. Qin, C. Jiang, J.W. Anderegg, C.J. Jenks, B. Gleeson, D.J. Sordelet, and P.A. Thiel, Surf. Sci. 601 (2007) 376-380.

6. Y. Cadoret, M.P. Bacos, P. Josso, V. Maurice, P. Marcus, and S. Zanna, Materials Science Forum, 461-464 (2004) 247-254.

7. P.Y. Hou and K.F. McCarty, Scripta mater., 54 (2006) 937-941.

8. P.Y. Hou and K. Priimak, Oxidation of Metals, 63 (2005) 113-129.

9. P.Y. Hou and V.K. Tolpygo, Surf. Coat. Technol., 27 (2007) 623-627.

10. D. Monceau et al., Oxid. Met., in press (2009).

11. A.B. Anderson, C. Ravimohan, and S.P. Mehandru, Surf.Sci., 183 (1987) 438-448.

12. R. Yu and P.Y. Hou, Appl. Phys. Lett., 91 (2007) 011907:1-3.

13. A. Gauffier, E. Saiz, A,P. Tomsia, and P.Y. Hou, J. Mater. Sci., 42 (2007) 9524-9528.

14. P.Y. Hou, Annu. Rev. Mater. Res. 38 (2008) 275-298.

15. L. Hu, D.Hovis, P.Y. Hou, J.L. Smialek, and A.H. Heuer, in preparation.

16. M.Y. He, A.G. Evans, and J.W. Hutchinson, Acta mater. **48**, 2593-2601 (2000).

17. J. L. Smialek, Met. Trans., 9A, (1978) 308.

18. J. L. Smialek, in N. L. Peterson Mem. Symp. Proc. on Oxidation and Associated Mass Transport, TMS-AIME, Warrendale, PA (1986) 297-313.

19. D. R. Sigler, Oxid. Met., **40** (1993) 555-583.

20. M.A. Smith, W.E. Frazier, and B.A. Pregger, Mat. Sci. Eng., 203 (1995) 388.

21. R. Janakiramanan, G.H. Meier, and F.S. Pettit, Met.Trans., 30A (1999) 2905-2913.

22. J.L. Smialek, "Moisture-Induced Delayed Spallation and Interfacial Hydrogen Embrittlement of Alumina Scales," NASA TM 2005-214030, 29 pages (Dec., 2005).

23. J.L. Smialek, Mater. Sci. Forum, 595-598 (2008) 191-198.

24. D.R. Clarke, R.J. Christensen, and V. Tolpygo, Surf. Coat. Technol., 94-95 (1997) 89-93.

25. J.L. Smialek and G.N. Morscher, *Mat. Sci. Engineer.* A **332** (2002) 11-24.

26. V. Tolpygo, D.R. Clarke, Mater. Sci. Eng. A278 (2000) 142–161.

27. V. Sergo and D.R. Clarke, J. Am. Ceram. Soc., **81** [12] (1998) 142-161.

28. X. Peng and D.R. Clarke, J. Am. Ceram. Soc., **83**, [5] (2000) 1165-1170.

29. J.L. Smialek, "Scale Adhesion, Sulfur Content, and TBC Failure on Single Crystal Superalloys," in Ceramic Engineering and Science Proceedings, American Ceramic Society, Westerville, OH, **23**, 4 (2002) 485-495.

30. J.L. Smialek, J. Therm. Spray Technol., 13 (2004) 66-75.

31. J.L. Smialek, Dongming Zhu, and Michael D. Cuy, Scripta Materialia, **59** (2008) 67-70; also "Moisture-Induced Delamination Video of an Oxidized Thermal Barrier Coating," NASA TM 2008-215210, (April, 2008).

32. M. Rudolphi, D. Renusch, and M. Schütze, *Scripta mat.*, 59 (2008) 255-257.

33. Y. Cadoret, A. Raffaitin, "Development and Use of High Temperature Coatings and TBC Bond Coats for Gas Turbine Engines," presented at Workshop on High Temperature Corrosion and Protection for Aeronautic Applications, D. Monceau, Chair, U. Toulouse, May 16, 2008.

34. J.L. Smialek, unpublished research, NASA Glenn Research Center, 2009.

35. M.C. Maris-Sida, G.H. Meier, and F.S. Pettit, Met. Trans., 34A (2003), 2609-2619

36. J.A. Nesbitt and J.L. Smialek, unpublished research, NASA Glenn Research Center, 2008

37. J.L. Smialek and A. Garg, unpublished research, NASA Glenn Research Center, 2009.

38. B.A. Pint, J.A. Haynes, Y. Zhang, K.L. More, and I.G. Wright, Surf. Coat. Tech. 201 (2006) 3852-3856.

39. D. Monceau and D. Ponquillon, Oxid. Met. 61 (2004) 143.

40. V. K. Tolpygo and D.R. Clarke, and K.S. Murphy, Surf. Coat. Technol., 146-147 (2001) 124-131.

41. S.T. Shiue, H.C. Lin, T.Y. Shen, and H.C. Hseuh, Mat. Sci. Eng. A 434, (2006) 202-206.

42. J.H. Keenan, F.G. Keyes, P.G. Hill, J.G. Moore, Steam Tables: Thermodynamic Properties of Water Including Vapor, Liquid, and Solid Phases, Wiley New York, 1978.

43. J.L. Smialek, JOM, (2006) **1**, 29-36.

44. V. Kucera and E. Mattson, "Atmospheric Corrosion," in *Corrosion Mechanisms*, F. Mansfield, ed., Marcel Dekker, New York, (1989) 211-284.

45. V.K. Tolpygo and D.R. Clarke, Acta mater. 46 (1998) 5153.

46. V. K. Tolpygo and D.R. Clarke, Acta mater. 48 (2000) 3283-3293.

47. V.K. Tolpygo and D.R. Clarke, Acta mat. 2004 (52), I and II, 5115-5141

48. Y. Zhang, J.A. Haynes, B.A. Pint, I.G. Wright, and W.Y. Lee, Surf. Coat. Technol., 163-164 (2003) 19-24.

49. M.W. Chen, R.W. Ott, T.C. Hufnagel, P.K. Wright, and K.J. Hemker, Surf. Coat. Technol., 163-164 (2003), 25-30.

50. D. Pan, M.W. Chen, P.K. Wright, and K.J. Hemker, Acta Mat. 51 (2003) 2205-2217.

51. V.K. Tolpygo and D.R. Clarke, Surf. Coat. Technol., 163-164 (2003), 81-86.

52. V. K. Tolpygo and D.R. Clarke, Surf. Coat. Technol., 200 (2005) 1726-1281.

53. S. Sridharan, L. Xie, E.H. Jordon, M. Gell, and K.S. Murphy, Mat. Sci. Eng., A393, (2005) 51-62.

54. M. Wen, E.H. Jordon, and M. Gell, Surf. Coat. Technol., 201 (2006) 3289-3298.

55. N. Vialas and D. Monceau, I, Oxid. Met. 66 (2006) 155-189: II, Oxid. Met., 68 (2007) 223-242.

56. K.S. Murphy, Howmet Corp., private communication, 2008.

Tolpygo-Murphy-Clarke, Acta mat. 2008 (56), 489-499.

Pint, Haynes, More, Wright in: Green KA, Pollock TM, Harada H, Howson TE, Reed RC, Shirra JJ, Walston S, editors. Superalloys 2004: The Minerals, Metals and Materials Society, 2004. p. 597

Figure Captions

Figure 1. SEM micrograph of as-coated Ni(Pt)Al surface showing grain boundary ridges, surface striations, and pits.

Figure 2. EDS response from overall, grain center (X), and grain boundary (Y) of figure 1.

Figure 3. Total cyclic oxidation weight change results for a Pt-aluminide coating on CMSX4. $1150^{o}C$, for 2000 1-hr cycles; 20 min. cooling cycle; held for up to 1 day to record weights. (Sample 1150-2 distinguished by excessive coating grain boundary wrinkling and local scale spallation compared to the more flat sample 1150-4 and minimal spalling).

Figure 4. Additional spallation recorded (cumulative), after the initial measurement, during hold times at ambient laboratory conditions. Delayed spallation became appreciable for sample 1150-2, beginning at about 750 cycles, but remained negligible for 1150-4. The sequential drops in weight at 2000 cycles occurred over a 24 hr period, followed by exposure to moisture and water immersion for 1 hr.

Figure 5. Degree of delayed spallation for each individual weighing period. On average, 0.04 mg/cm^2 additional spalling for 1150-2; no (0.00 mg/cm^2) additional spallation for 1150-4.

Figure 6. Time dependency of delayed spallation for sample 1150-2 measured after various oxidation test times. (Time, weight axes relative to first weight measurement). In some cases, additional spallation continued past 5 hr to at least 1 day after cooling. (Occasionally, residual warmth from the cooled samples produced electronic drift and an apparent weight gain for 1-2 minutes in the microbalance).

Figure 7. Minimal time dependent delayed spallation for sample 1150-4 at various cycle times. (Time, weight axes relative to first weight measurement). Very little additional spallation continued past 1 hr.

Figure 8. Optical macrographs, obtained under oblique lighting, showing a) rough surface topography of the coating grains for sample 1150-2; and b) comparatively flat coating for sample 1150-4. (200 1-hr cycles to $1150^{o}C$).

Figure 9. Optical micrographs showing a) detached alumina scale and exposed metal associated with deep grain boundary undulations for sample 1150-2; and b) comparatively flat coating surface and mostly adherent scale for sample 1150-4. (at 200, 500, and 1000 1-hr cycles to $1150^{o}C$).

Figure 10. Optical macrographs showing a) appreciable spalling (arrow) to bare metal for sample 1150-2; and b) minimal spallation (arrow) for sample 1150-4; both before and after water immersion for 1 hr. (2000 1-hr cycles to $1150^{o}C$).

Figure 11. Backscatter SEM micrographs of (a) sample 1150-2 showing large 500 μm area of spalling to bare metal and mottled regions of intact oxide; and (b) sample 1150-4 showing relatively uniform, attached, but cracked scale. (2000 1-hr cycles to $1150^{o}C$).

Figure 12. EDS spectra for bright exposed metal and grey spinel scale features of sample 2 and overall uniform alumina scale on sample 4 (from Figure 11).

Figure 13. Temperature dependence of water vapor pressures at saturation and typical relative humidity levels. Saturation values and moisture contents at the ambient, balance conditions (A) compared to saturation values for the cooling chamber (B). A relative humidity of 85% at ambient temperature translates to 2.1% at 100°C.

Grain Boundary Ridges in As-Received Ni(Pt)Al Coating
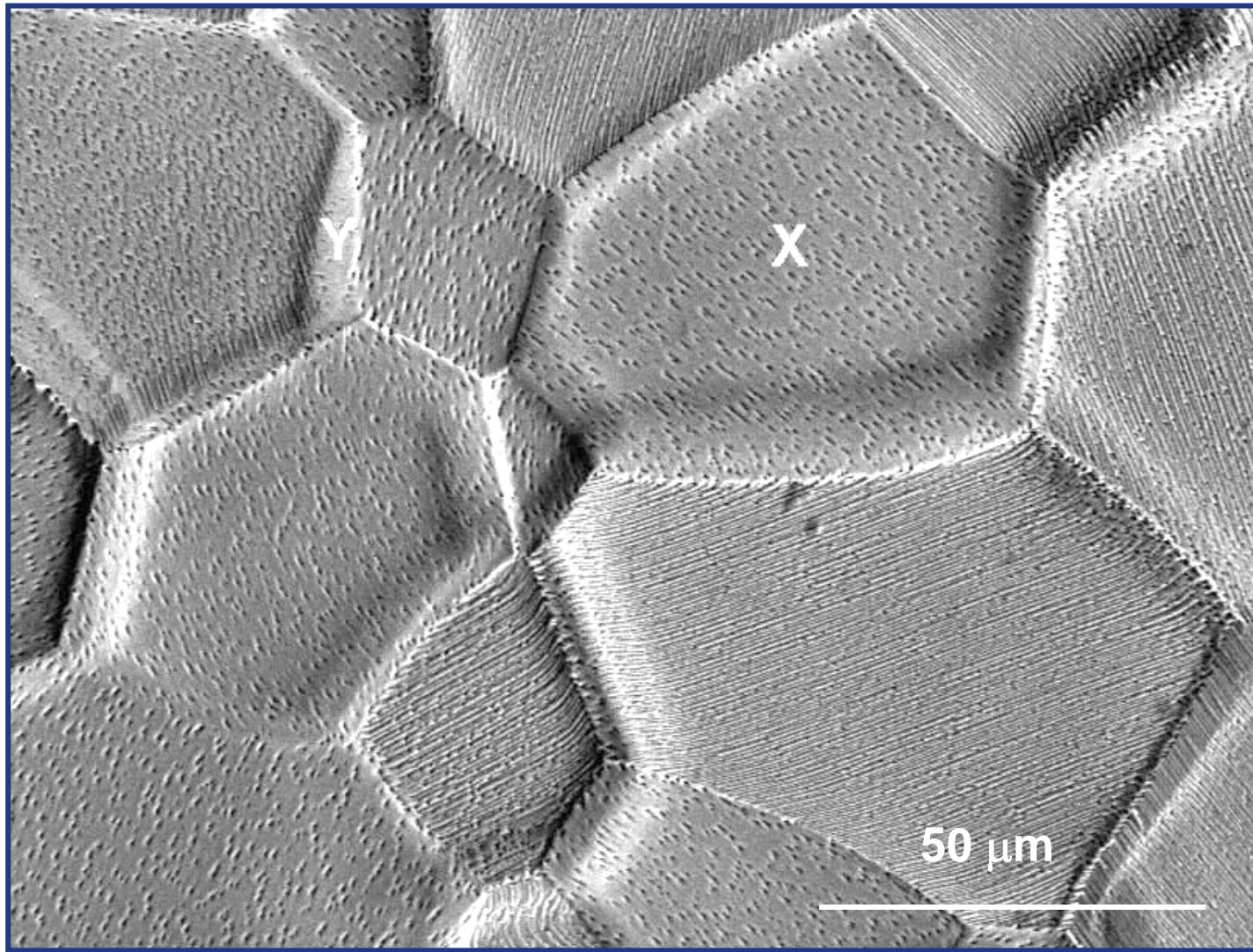
Ni, Al, Pt coating surface with (Cr, Fe, Co)

Y grain boundary

X grain center

Ni Al Pt   Cr Fe Co

500x overall
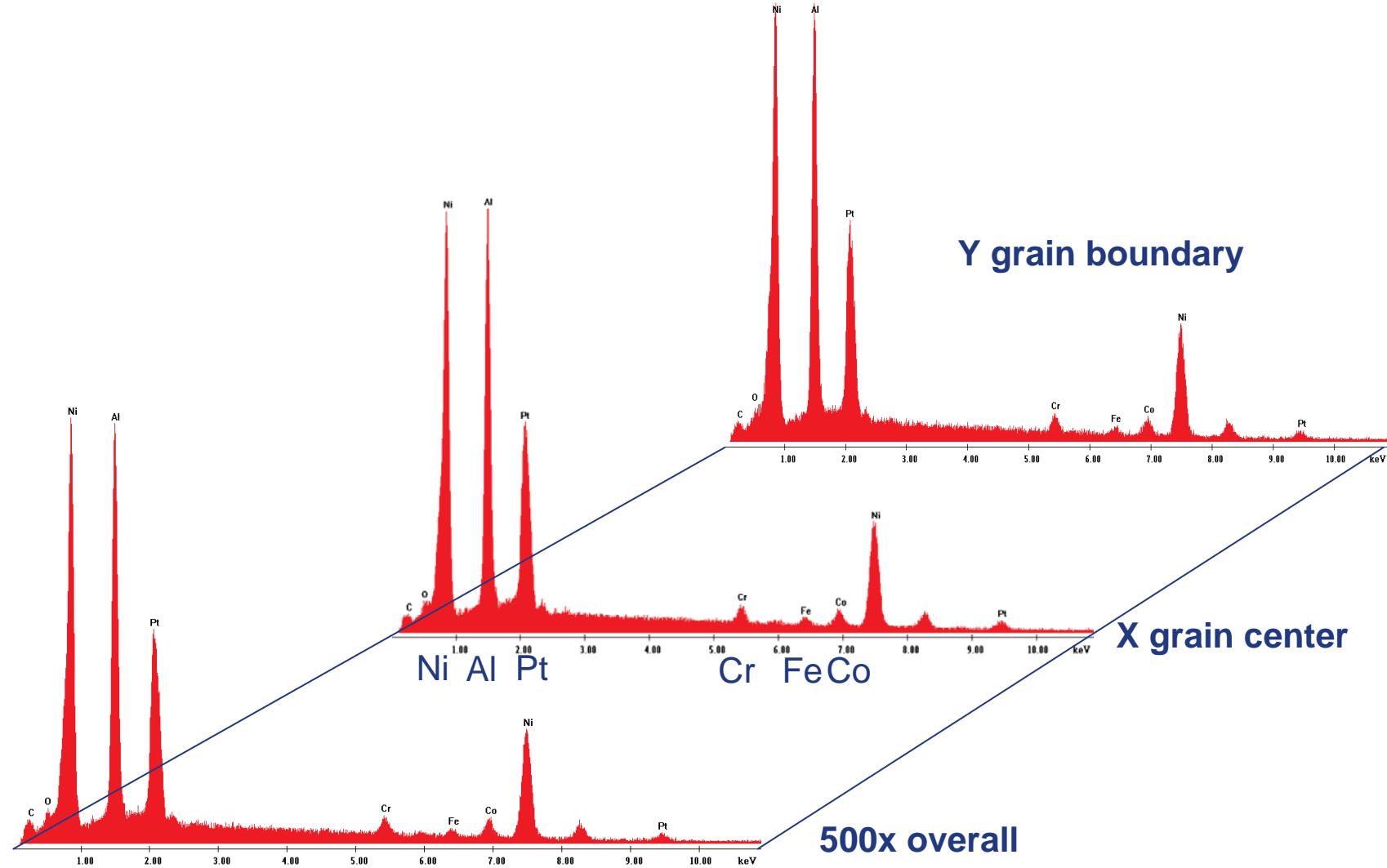
Total Weight Change

1150°C Cycling Ni(Pt)Al on CMSX4

1 hr. heat , 20 min. cool, plus 1 min. - 1 day @ ambient
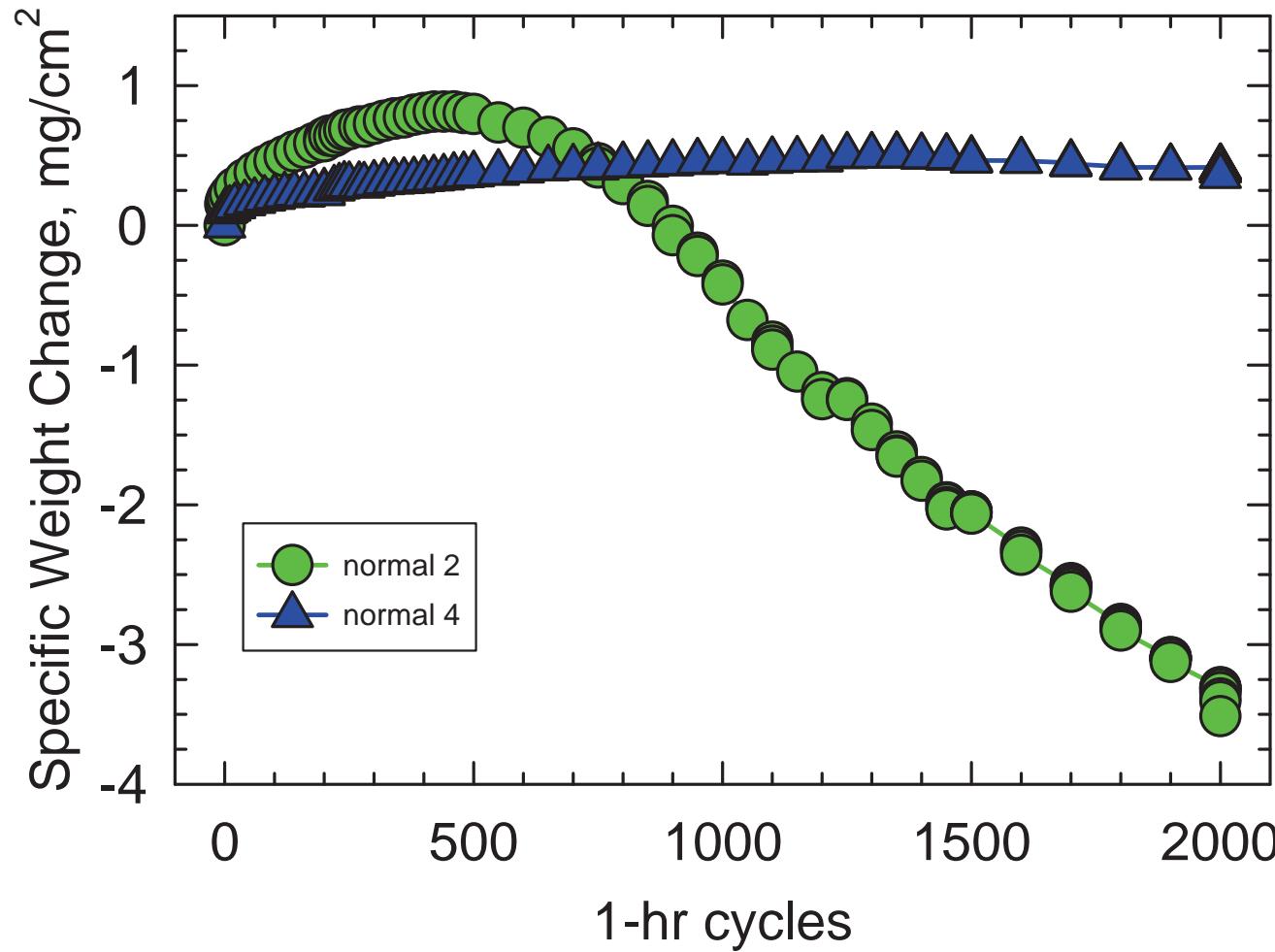
Cumulative Delayed Spallation

1150°C Cycling Ni(Pt)Al on CMSX4
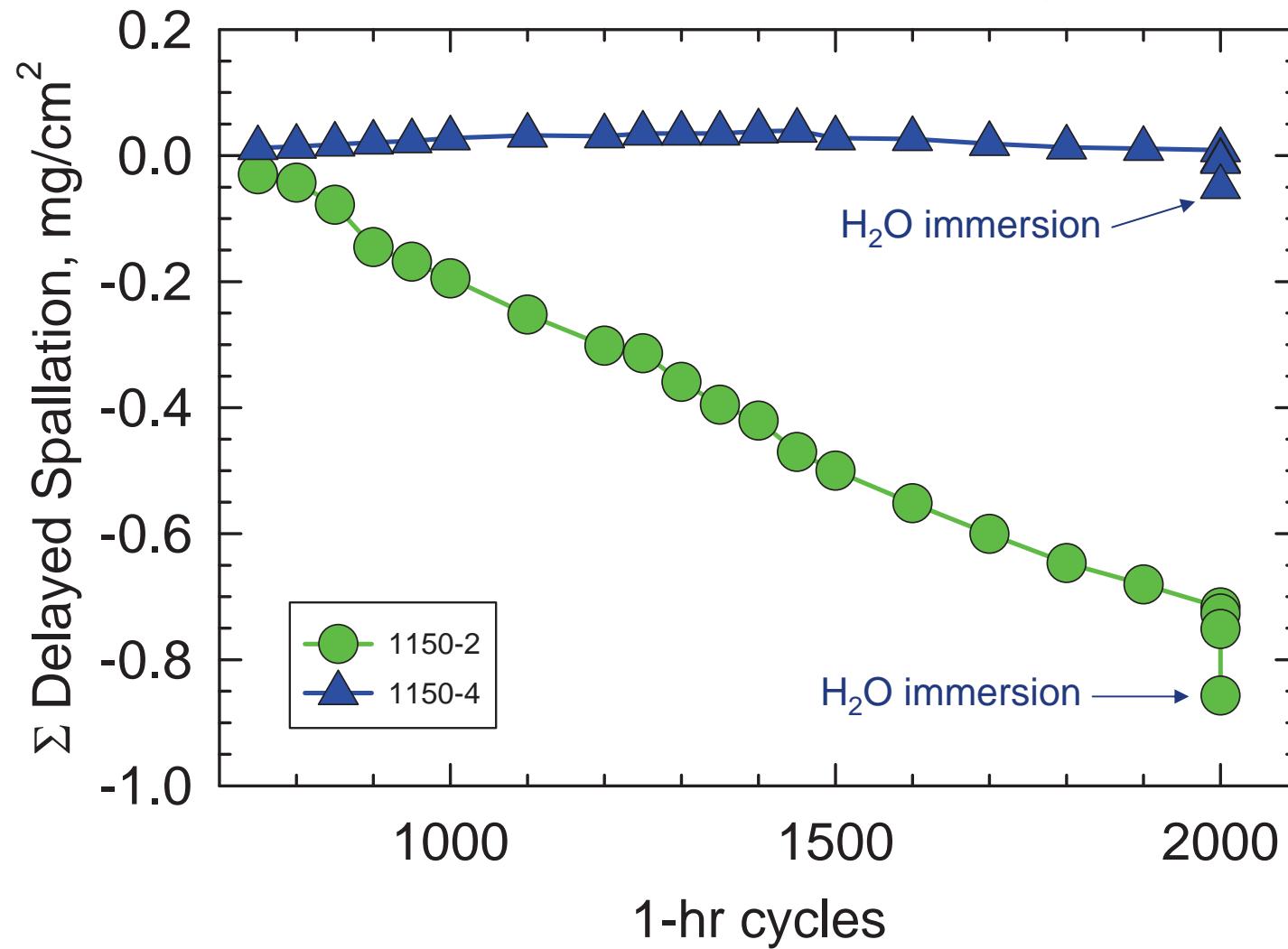
1 hr. heat , 20 min. cool, plus 1 min. - 1 day @ ambient

Delayed Spallation after 1150°C Cycling
Ni(Pt)Al on CMSX4
1 hr. heat , 20 min. cool, plus 1 min.-1 day @ ambient
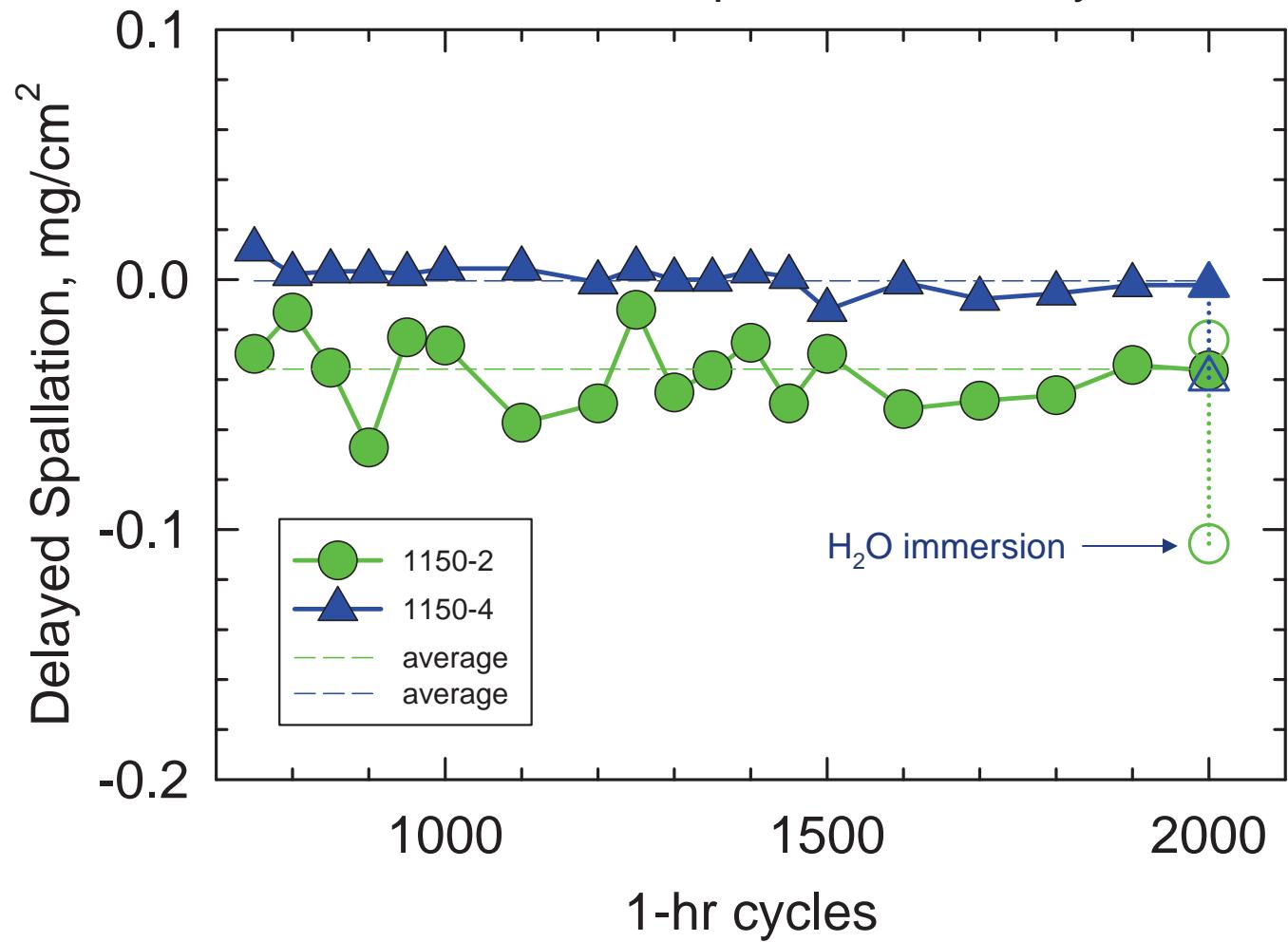
Delayed Spallation after 1150°C Cycling

Ni(Pt)Al on CMSX4; 1150-2

1 hr. heat , 20 min. cool, plus 1 min.-1 day @ ambient
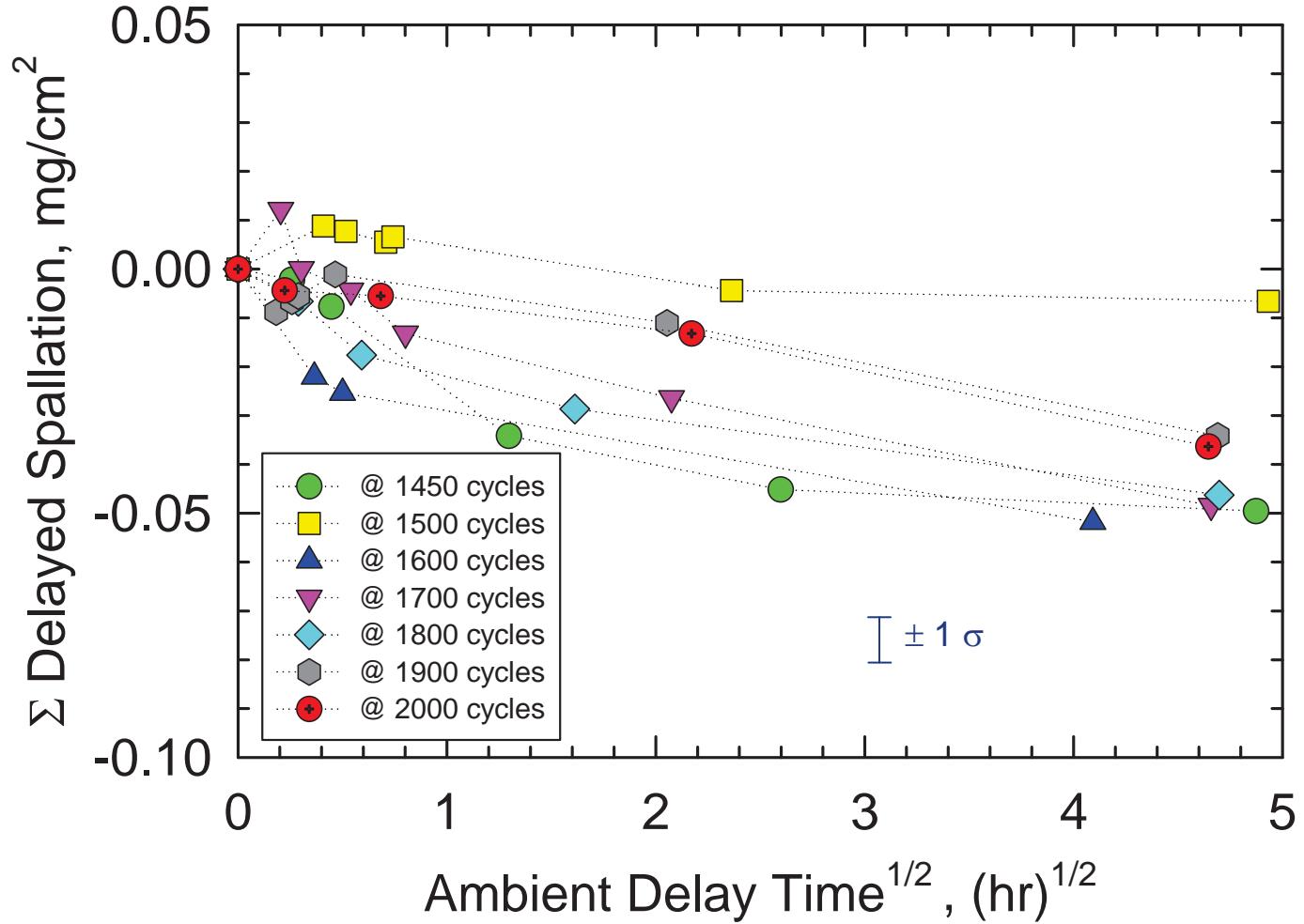
Delayed Spallation after 1150°C Cycling

Ni(Pt)Al on CMSX4; 1150-4

1 hr. heat , 20 min. cool, plus 1 min.-1 day @ ambient
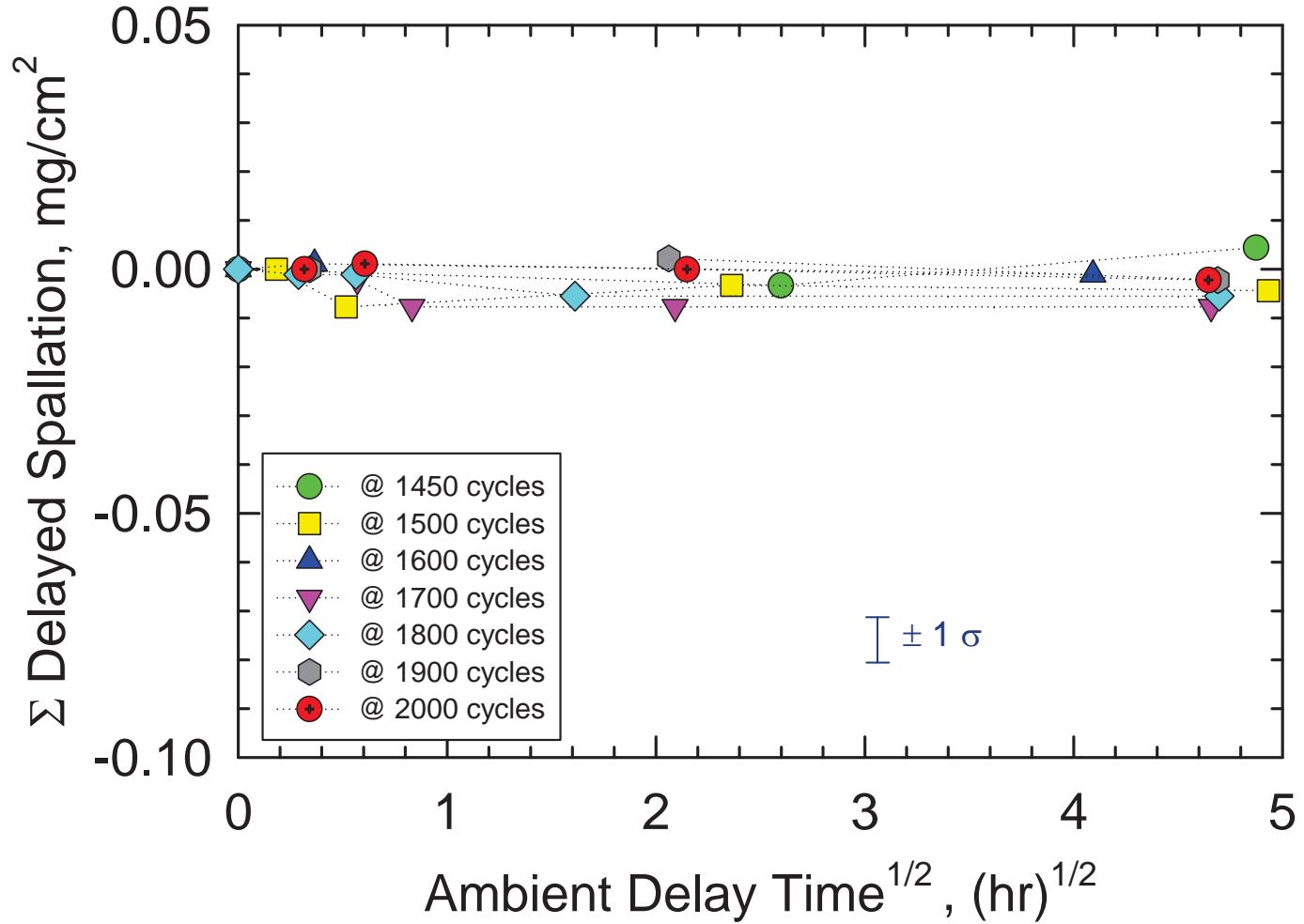
Surface Macrostructure of Ni(Pt)Al Coating
200 1-h cycles @ 1150°C; oblique lighting; 50x

1150-2

1 mm

1150-4

200 hr

metal

Al$_2$O$_3$

500 hr

metal

1000 hr

Al$_2$O$_3$→

0.2 mm
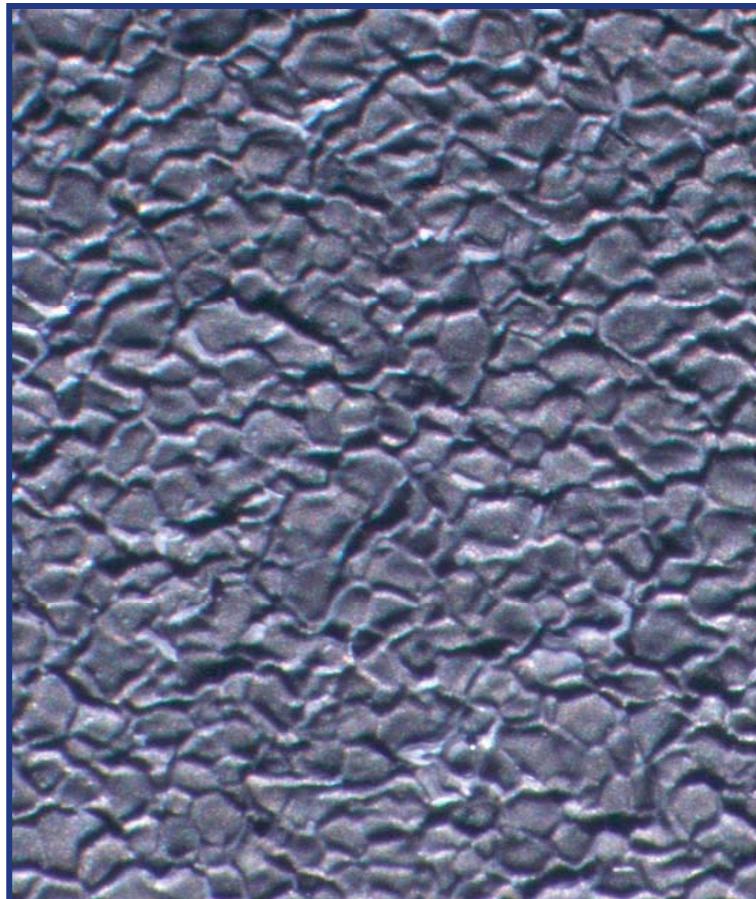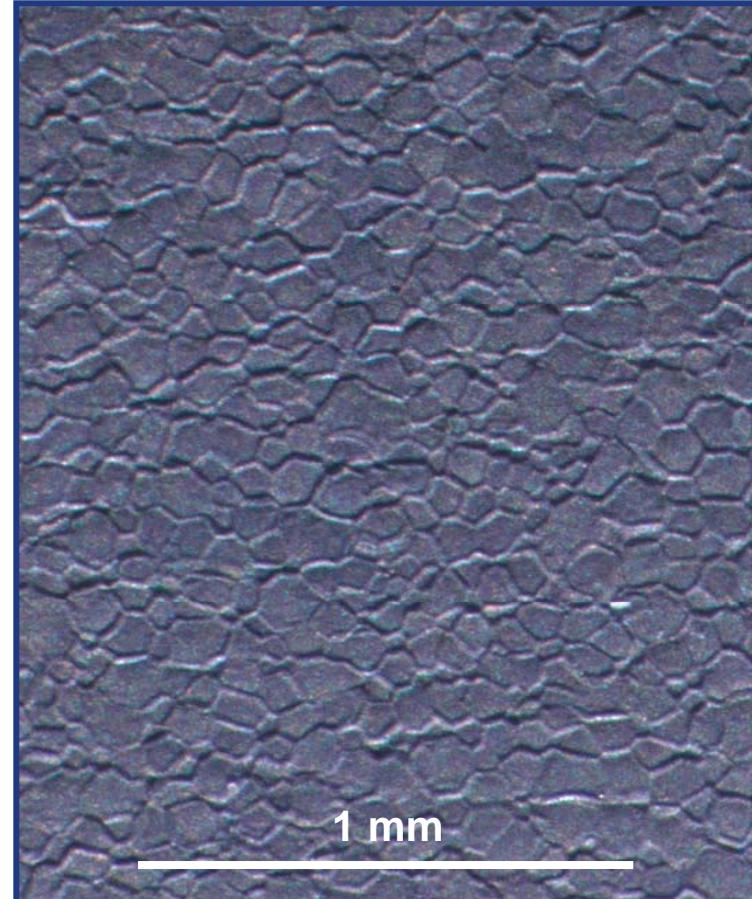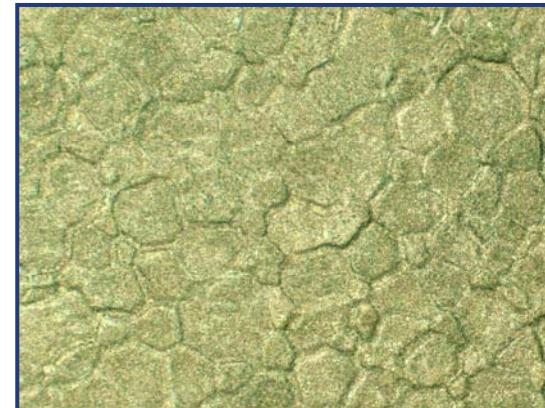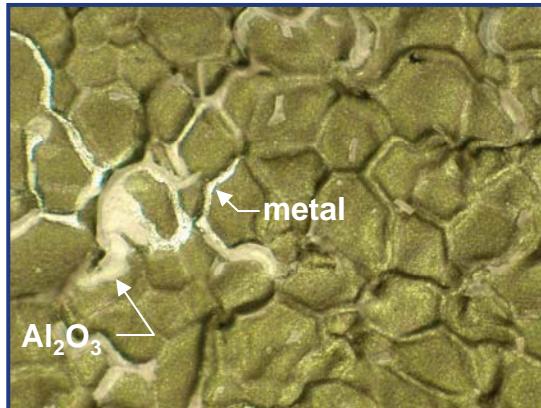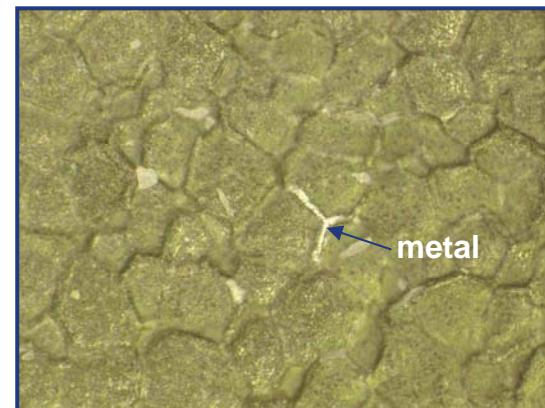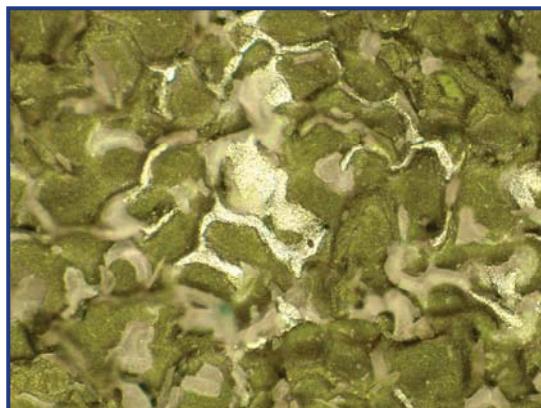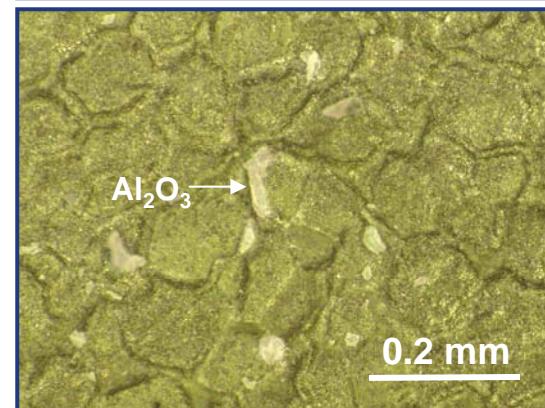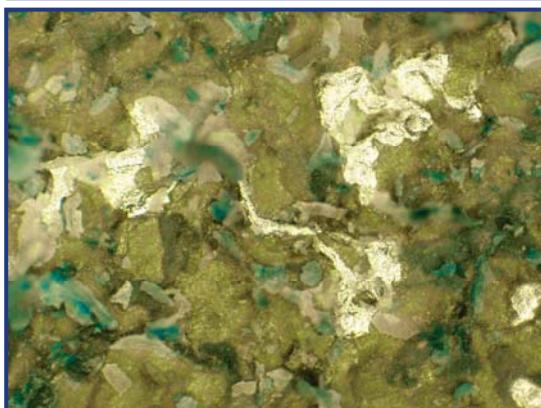
1150-2

1150-4

Contrasting Spallation Patterns Before/After Water Immersion
Ni(Pt)Al Coating; 2000 1-h cycles @ 1150°C; 25x

Before

After

1150-2   1150-4

1 mm
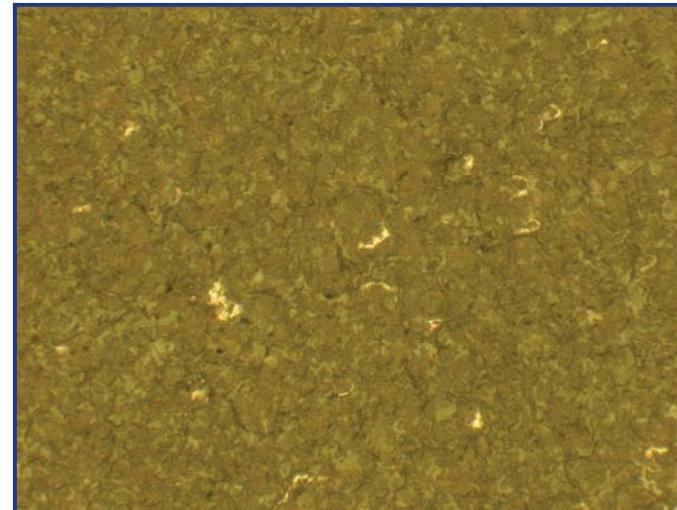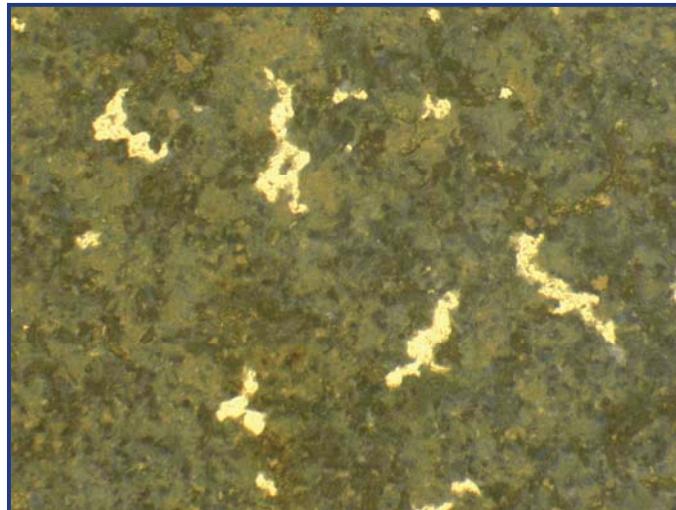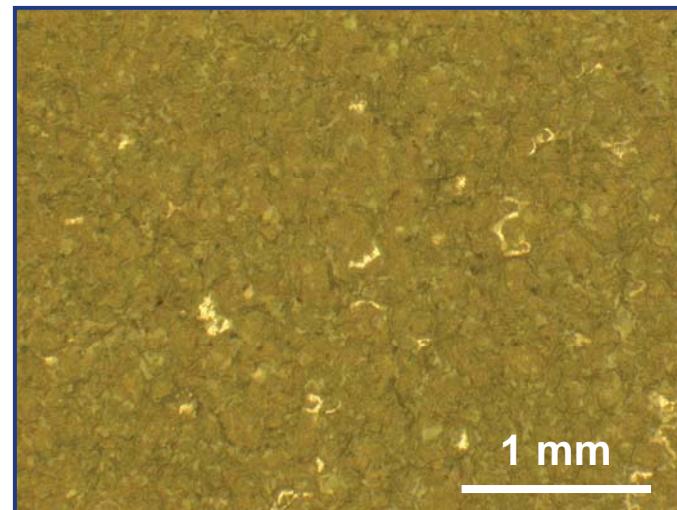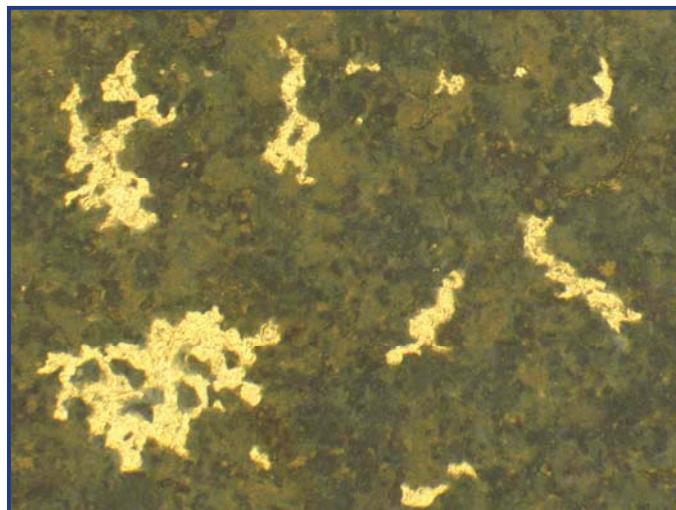
# Spallation Differences
1150-2, 4 after 2000 1-hr cycles; BSE
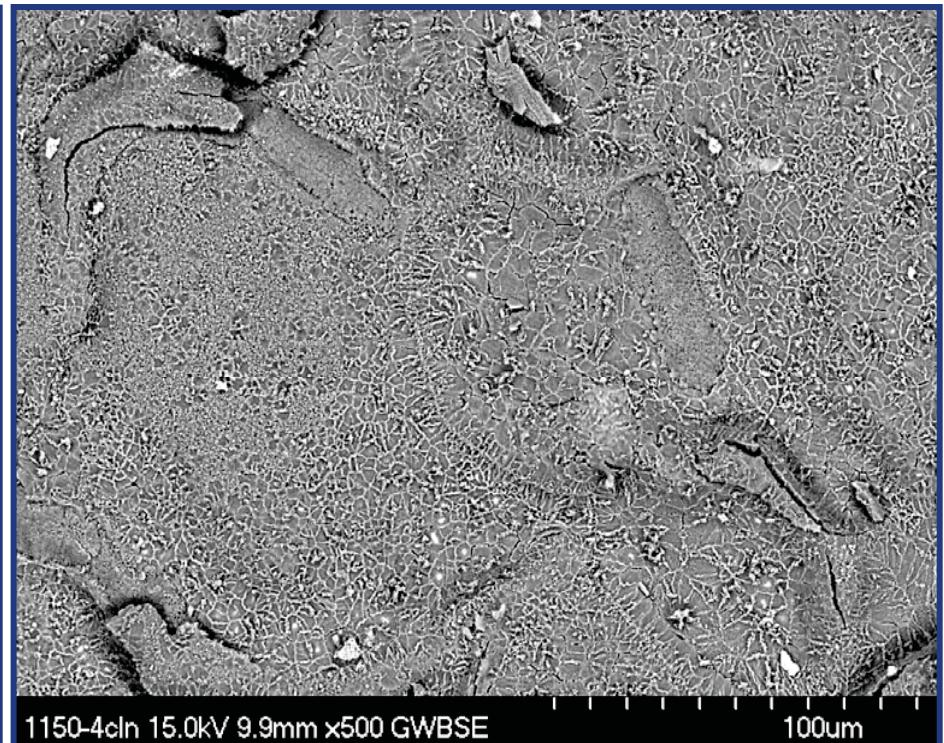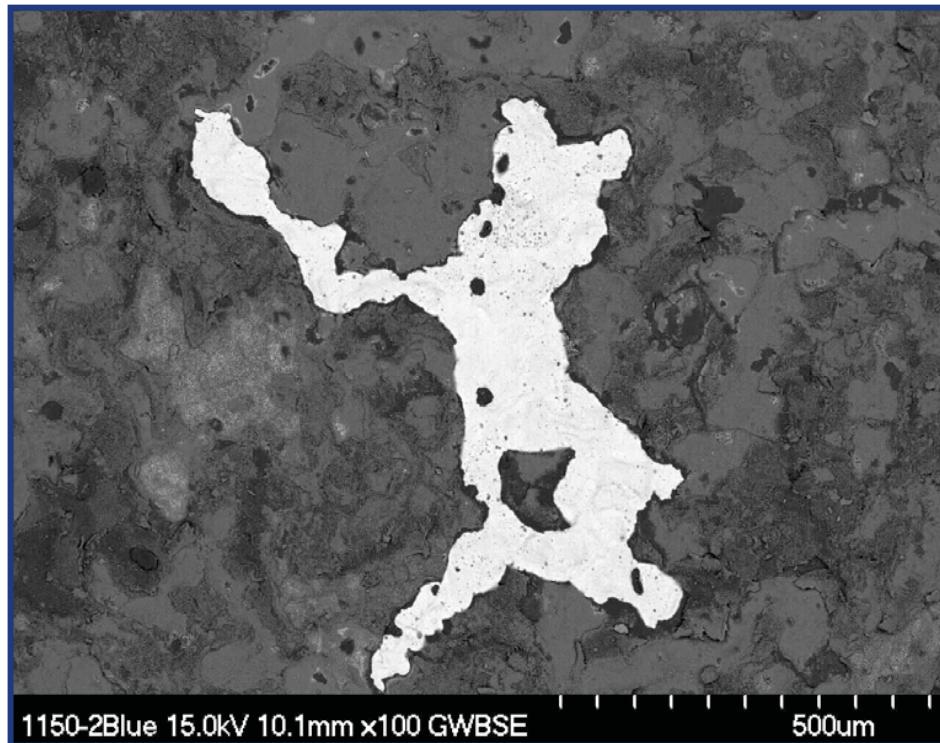
1150-2

1150-4

EDS Spectra of 1150-2 Exposed Metal, Faceted Spinel, and 1150-4 Uniform Alumina Scale Regions

Al_2O_3

$NiAl_2O_4$

Bare metal

O Ni Al W Pt   Ti   Cr   Co Ni
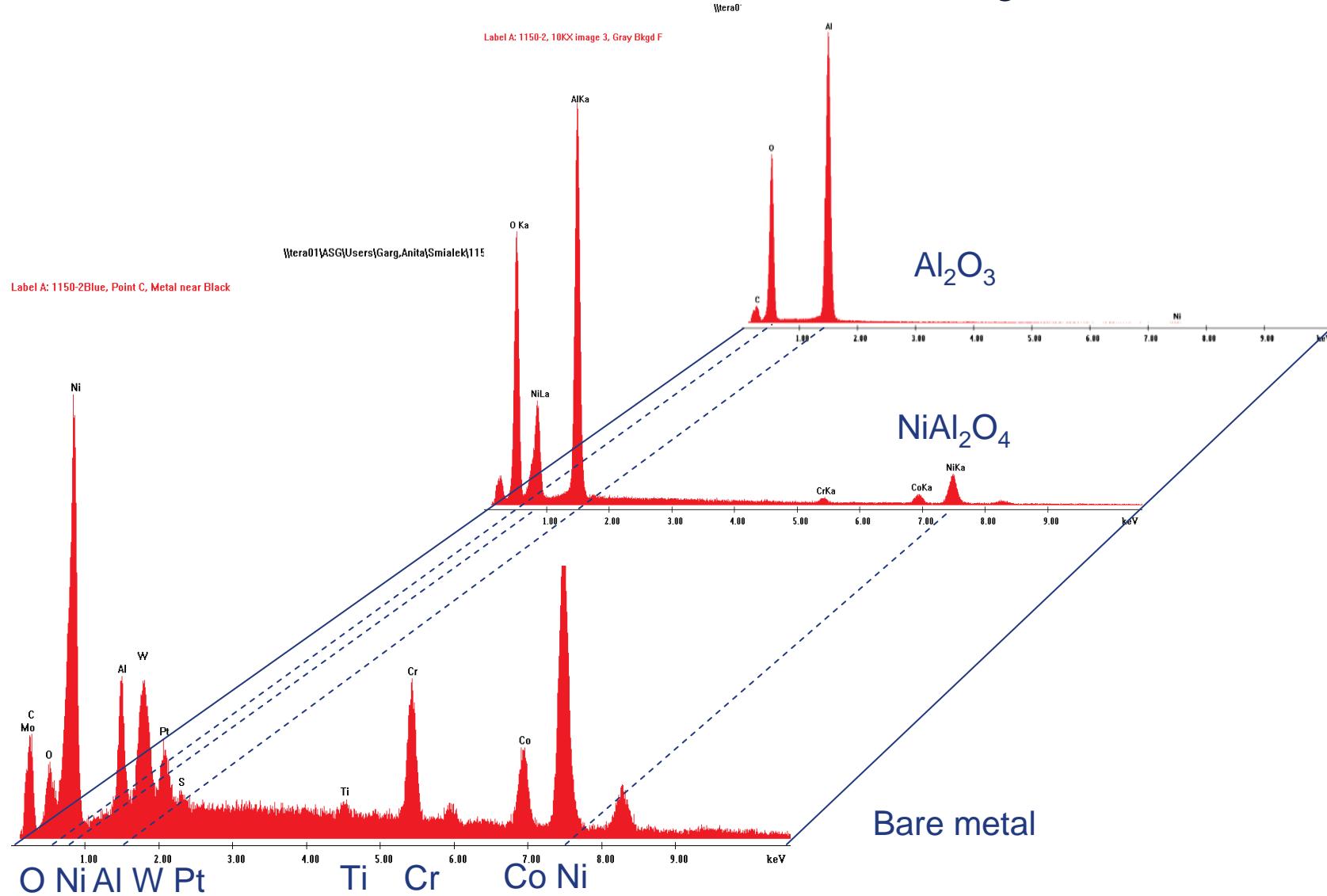
Saturation Vapor Pressure and Relative Humidity